Chemical Vapor Deposition

DOI: 10.1002/cvde.200806708

Full Paper

Study of Atmospheric MOCVD of TiO_2 Thin Films by Means of Computational Fluid Dynamics Simulations**

By *Neyda Baguer*,* *Erik Neyts*, *Sake Van Gils*, and *Annemie Bogaerts*

This paper presents the computational study of the metal-organic (MO) CVD of titanium dioxide (TiO_2) films grown using titanium tetraisopropoxide (TTIP) as a precursor and nitrogen as a carrier gas. The TiO_2 films are deposited under atmospheric pressure. The effects of the precursor concentration, the substrate temperature, and the hydrolysis reaction on the deposition process are investigated. It is found that hydrolysis of the TTIP decreases the onset temperature of the gas-phase thermal decomposition, and that the deposition rate increases with the precursor concentration and with the decrease of substrate temperature. Concerning the mechanism responsible for the film growth, the model shows that at the lowest precursor concentration, the direct adsorption of the precursor is dominant, while at higher precursor concentrations, the monomer deposition becomes more important.

Keywords: Atmospheric pressure, MOCVD, Simulation, TiO_2 films, TTIP

1. Introduction

Titanium dioxide (TiO_2) films are widely used in industrial applications due to their optical, chemical, and electrical properties. TiO_2 films have a high refractive index and high dielectric constant; they are transparent in the visible and near infrared range, chemically stable. and non toxic.[1] Therefore they can be used as a pigment[2] and UV filter in the cosmetic industry, as an antireflective coating[3] in the glass industry, and as a dielectric material for integrated circuits.[4] TiO_2 films have also found applications in the production of solar cells,[5] as well as in catalysis and photocatalysis[6] as, for example, in the destruction of organic materials.[7,8]

TiO_2 films can be prepared by various techniques, e.g., sputtering,[9] evaporation,[10] atomic layer deposition,[11] and CVD.[7,8,12–14] Among these, MOCVD[15–17] is a low cost technique, which allows controlling the microstructure and the stoichiometry of the films, while permitting large areas to be treated.

MOCVD can be operated in a wide range of pressure, temperature, and precursor concentrations. However, the combination of these parameters determines the quality of the film and therefore it is useful to predict under which conditions the most desirable deposition can be achieved. This can be accomplished with the help of computer simulations.

In the present work, the influence of the precursor concentration and substrate temperature on the deposition and growth of TiO_2 films resulting from atmospheric MOCVD of titanium tetraisopropoxide, $Ti(OC_3H_7)_4$ (TTIP), is investigated. Moreover, the influence of the hydrolysis reaction on the onset temperature of the gas-phase thermal decomposition is studied by means of computational fluid dynamics (CFD) simulations, using a commercially available code, "FLUENT".[18] Experimental studies on atmospheric MOCVD for depositing TiO_2 films from TTIP using (horizontal) hot-wall reactors have been reported in the literature.[15,17] In other work, a cold-wall reactor, operating under conditions very similar to the present study, was investigated.[19] Concerning theoretical investigations, most of the MOCVD processes have been modeled at low pressure. For example, the sintering of TiO_2 particles on hot-wall reactors has been modeled,[20] while TiO_2 film deposition on a cold-wall reactor has also been dealt with.[21,22] In a previous study,[23] we have simulated atmospheric MOCVD, and the effect of substrate temperature on the deposition rate was investigated under a fixed precursor partial pressure. In the present paper special attention is paid to the role of the substrate temperature,

[*] Dr. N. Baguer, Dr. E. Neyts, Prof. A. Bogaerts
Research group PLASMANT, Department of Chemistry, University of Antwerp (UA) Universiteitsplein 1, B-2610 Antwerp (Belgium)
E-mail: neyda.baguer@ua.ac.be
Dr. S. Van Gils
OCAS, Arcelor Research Industry Ghent, Surface Functionalisation John Kennedylaan 3, B-9060 Zelzate (Belgium)
Dr. S. Van Gils
FLAMAC (Flanders Materials Centre)
Technologiepark 903, B-9052, Zwijnaarde (Belgium)

[**] This work was supported by the Flanders Materials Center (FLAMAC) and the IWT. The authors would like to thank D. Autrique (UA) for his advice on the use of Fluent, and A. Martin (FLAMAC) and G. Huybrechts (UMICORE) for all the interesting discussions.

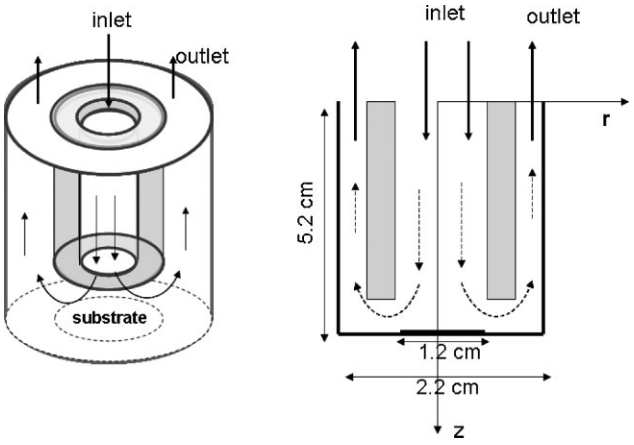

Fig. 1. Geometry of the CVD reactor and its schematic representation.

precursor concentration, and TTIP hydrolysis reaction on the deposition process.

2. Description of the Model

The simulations were carried out for a cold-wall, plug-down vertical reactor (see Fig. 1 below). The gas mixture was assumed to be uniform. The flow was considered laminar and since the film growth rate was slow compared to the flow velocity, a steady state was assumed as well. The homogeneous and heterogeneous reactions considered in the model were the same as in the literature, [23] i.e., thermal decomposition,[24] hydrolysis,[20] and surface deposition[25] of TTIP vapor, as well as the surface deposition[13,23] of TiO_2 monomers. These reactions are listed in Table 1. The reaction rate constants were calculated through the Arrhenius expression, and the corresponding activation energies and pre-exponential factors are tabulated as well. Note that there were two volumetric and two surface reactions. These reactions were considered to occur only in the right direction, i.e., they were far from equilibrium, because CVD reactors can not operate at equilibrium, as they continuously produce a net change of reactant to product.

The transport and chemistry present in the CVD processes were simulated by solving the conservation equations for the mass, momentum, energy, and chemical species. The differential equations were discretized using the finite volume method.[26] The obtained system of algebraic equations was solved iteratively and semi-implicitly using the pressure-based segregated solver in which the governing equations were solved sequentially, (i.e., ''segregated'' from one another) in each time iteration. In this solution method, the pressure equation was derived from the continuity and momentum equations in such a way that the velocity, corrected by the pressure, satisfied the continuity equation, i.e., following the projection method.[27] For this pressure-velocity coupling the Simple method[28] was selected, and the second order upwind Scheme [29] was used to interpolate the variables on the surface of the control volume. Together with the pressure-based segregated solver, the so-called ''stiff chemistry'' solution procedure[30] was used, which allows solving the chemistry and the transport equations decoupled in time. This was necessary because the hydrolysis reaction had a very high reaction rate, and hence its reaction time scale was much faster than the convection and diffusion time scale, which makes the solution of the transport equations numerically difficult.

Due to the axial symmetry of the reactor, the fundamental equations of the fluid dynamics were solved in two-dimensions in a mesh system of 5939 node points, in which the size of the grids was refined in the region close to the substrate. Indeed, a larger gradient in temperature and species concentration was expected in this region. In order to solve the system of equations in the computational domain the following boundary conditions were assumed for the reactor walls and the gas flow. A constant temperature at all the reactor walls and the substrate was assumed. Moreover, for the flow, the velocity, the temperature, and the chemical species mass fractions were defined at the reactor inlet, while at the outlet, an overall mass balance correction and zero diffusion flux in the direction normal to the exit plane were assumed for all the flow variables. The set of thermochemistry data used in the calculations for all the chemical species and the gas mixture is provided in the Appendix. A schematic diagram of the simulated reactor is shown in Figure 1.

3. Results and Discussion

The simulation results presented here correspond to the MOCVD of titanium dioxide films grown using TTIP as a source precursor, and nitrogen as a carrier gas. The TiO_2

Table 1. Chemical reactions considered in the model, as well as the activation energy and pre-exponential factors used to calculate their rate constants.

	Reactions	Classification	Activation energy [kJ mol^{-1}]	Pre-exponential factor [s^{-1}]	Ref.
1	$Ti(OC_3H_7)_4 \rightarrow TiO_2(g) + 4C_3H_6 + 2H_2O$	volumetric	70.5	3.96×10^5	[22]
2	$Ti(OC_3H_7)_4 + 2H_2O \rightarrow TiO_2(g) + 4C_3H_7OH$	volumetric	8.43	3.0×10^{15}	[18]
3	$Ti(OC_3H_7)_4 \rightarrow TiO_2(c) + 4C_3H_6 + 2H_2O$	surface	126.01	1.0×10^9	[23]
4	$TiO_2(g) \rightarrow TiO_2(c)$	surface	126.01	1.0×10^9	[11,21]

films were deposited under atmospheric pressure. The inlet gas (nitrogen + TTIP) temperature was set to 408 K, and its velocity to 0.368 m s^{-1}. The mole fraction of TTIP was varied between 10^{-3} and 10^{-5}. The reactor walls were considered temperature controlled, and a constant temperature of 408 K, which corresponds to the assumed inlet gas temperature, was assumed for the axial walls. For each value of the TTIP concentration, the substrate temperature was varied from 773 K to 973 K, which are typical conditions for the MOCVD of TiO_2 films using TTIP as the precursor. This arrangement allows the study of the effect of the precursor concentration and substrate temperature in the deposition process.

3.1. Analysis of the Gas Flow Profile

Figure 2a shows the gas velocity profile throughout the reactor. In the radial direction, the velocity reached its maximum at the axis and decreased toward the walls due to the viscous drag, i.e., a typical parabolic pattern, characteristic of laminar flows. In the axial direction the velocity increased upward until a layer was reached, close to the substrate, where the axial velocity became almost zero, i.e., until the velocity boundary layer.

In axisymmetric reactors, the concentration boundary layer can be taken equal to the velocity boundary layer, since this is where the flow stream begins to stagnate.[31] Hence from this distance it can be considered that the transport of reactants to the surface is no longer by convection, but by diffusion through a relatively stagnant boundary layer of gas. In the present reactor, we can consider that the transition from convective to diffusive transport occurred at a distance of around 1 mm from the substrate surface, as can be observed from the axial velocity profile shown in Figure 2b. The fact that the stagnant boundary layer was close to the substrate favored the uniformity of the film as the monomers had less time (volume) to nucleate and form particles in the gas phase before being carried away by the gas flow.

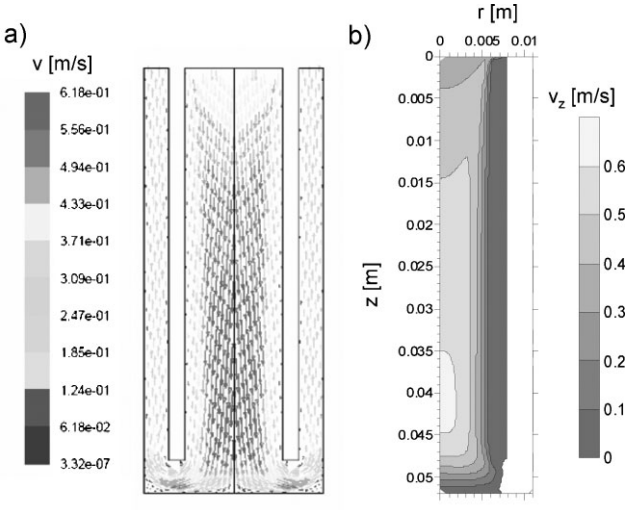

Fig. 2. a) Profile of the velocity vector colored by the speed magnitude, b) contour plot of the axial velocity, at 973 K and a TTIP mole fraction of 7.5×10^{-4}.

3.2. Temperature and Homogeneous Reaction Rates

The gas temperature throughout the reactor stayed constant at its inlet value (408 K) except at the region very close to the substrate, where a steep temperature gradient was present (see Fig. 3a).

Hence the occurrence of precursor decomposition was limited to that region (see Fig. 3b), as in the gas phase the depletion of TTIP was due to its thermal decomposition and hydrolysis reactions. By comparing the zoomed-in view contour lines of the temperature (Fig. 3c) and thermal decomposition rate (Fig. 3d), the onset temperature for this

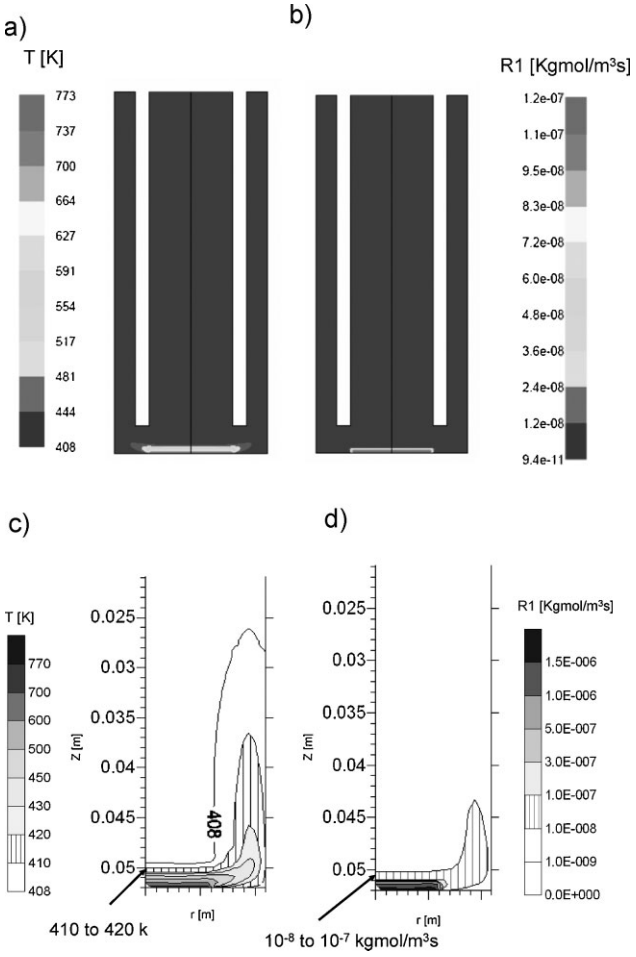

Fig. 3. Profiles of a) the temperature and b) thermal decomposition rate, and c), d) the corresponding detailed views, at a substrate temperature of 773 K and a TTIP mole fraction of 7.5×10^{-4}. Note that the contour line corresponding to 408 K, (i.e., the temperature of the gas at the inlet), is found at $z = 4.95$ cm, i.e., at a distance from the substrate surface of 2.5 mm.

process was estimated to be around 415 K. However this temperature does not necessarily indicate the onset temperature for the film growth as the surface reactions in Table 1 have higher activation energy, so they will probably only occur at higher temperature. In our previous work, the onset temperature for the film growth was estimated to be around 550 K.[23] In the literature it has been reported that the onset temperature for the film growth depends on whether or not TiO_2 has been previously deposited;[11,32] for example Komiyama[33] observed that the onset temperature for the surface decomposition of TTIP was around 523 K, in reactors where TiO_2 has been deposited earlier, and 643 K in reactors that were clean.

In previously reported work, based on IR measurements, precursor depletion near the substrate surface was observed and the gas-phase dissociation of TTIP was suggested to be a possible reason.[3] In order to check this assumption, additional simulations were carried out in which only the volumetric reactions were included. When comparing both calculations, it was concluded that the gas-phase reactions were slightly more important for the depletion of TTIP in the reactor at high substrate temperature, (i.e., around 55% for a substrate temperature of 973 K) but with decreasing the substrate temperature, the heterogeneous reactions became more important, and at 773 K they accounted for around 70% of the calculated TTIP depletion close to the substrate. These results are almost independent of the TTIP concentration at the reactor inlet at the range of TTIP concentrations investigated here.

The thermal decomposition of TTIP (reaction R1) gave rise to the production of water and TiO_2 monomers. As soon as water was present in the reactor, due to its oxidation effect on TTIP, hydrolysis occurred almost instantaneously (reaction R2), increasing even more the TiO_2 monomer population. The hydrolysis reaction of TTIP became predominant over the gas thermal decomposition under all conditions investigated, especially at higher precursor concentration (see Fig. 4). Hence close to the substrate

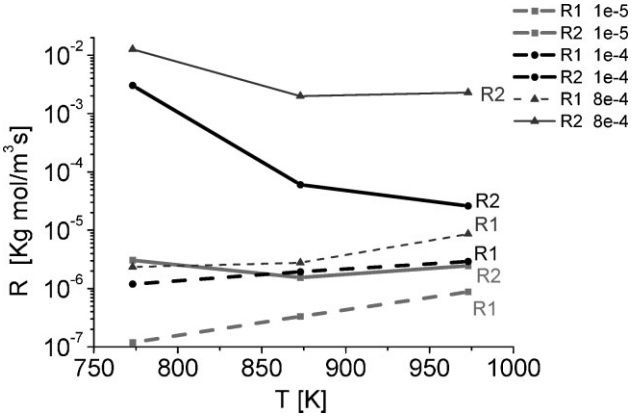

Fig. 4. Homogeneous reaction rates as a function of substrate temperature and for different TTIP mole fractions. The thermal decomposition (R1) and hydrolysis (R2) rates are represented by the dashes and solid lines, respectively.

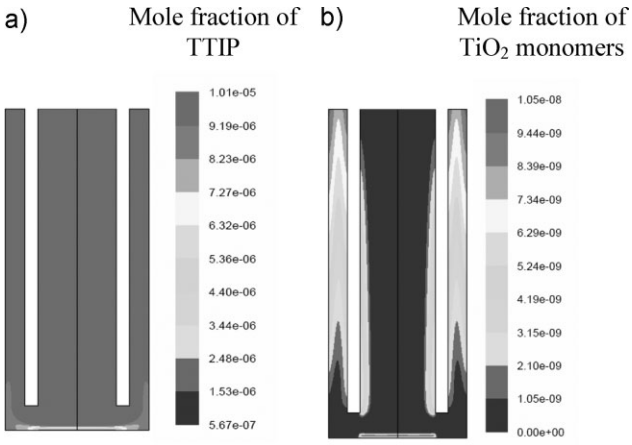

Fig. 5. Profiles of the a) TTIP and b) TiO_2 monomer concentrations at a TTIP mole fraction at the inlet of 10^{-5} and at a substrate temperature of 773 K.

surface, a steep mass density gradient was present, as can be seen from the TTIP and TiO_2 monomer mole fraction profiles presented in Fig. 5.

Throughout almost the entire reactor volume, the TTIP concentration stayed at the inlet mole fraction, which for the present case was equal to 10^{-5}, and consequently there was not any production of monomers. At a distance of around 1mm from the substrate surface, the precursor concentration began to decrease, reaching a minimum of 5.7×10^{-7} just in front of the substrate (see Fig. 5a) while the monomer mole fraction increased from zero to its maximum value of 1.05×10^{-8} (see Fig. 5b). This meant that at this condition, i.e., at the lower precursor concentration and substrate temperature, the mole fraction of TiO_2 in the gas represented only 0.1% of the mole fraction of TTIP which had been depleted in the reactor. On increasing the temperature and inlet precursor concentration this percentage increased, and at a TTIP inlet concentration of 7.5×10^{-4} and 973 K, the mole fraction of TiO_2 monomers in the gas flow represented 65% of the mole fraction of depleted TTIP. Hence the rest of the TiO_2 could either be deposited on the substrate or swept out from the reactor. A clarification for this can be found by investigating the mechanisms responsible for the surface deposition.

3.3. Surface Deposition

The deposition profile for all the conditions was found to be uniform as a function of the radial position, as is clear from Figure 6, except at the end of the substrate, which was an end-effect due to the reactor geometry (see Fig. 1).

The uniformity of the substrate deposition could be inferred from the temperature profile, where a gradient was only present very close to the substrate (i.e., 2.5 mm above the surface) and the contour lines of constant temperature were almost parallel to it (see Figs. 3a and 3c).

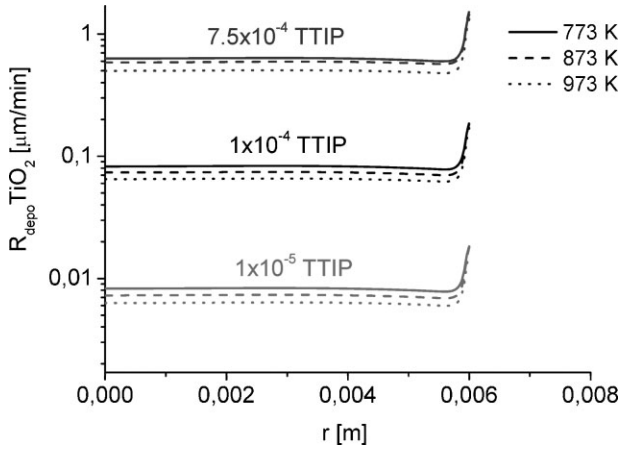

Fig. 6. Surface deposition rate as a function of radial position, for various substrate temperatures and precursor concentrations.

The importance of the different surface deposition mechanisms can be deduced from the ratio of the surface deposition rates, presented in Figure 7. It was found that at 10^{-5} mole fraction of the precursor, the direct adsorption of TTIP was almost completely responsible for the film growth (99% at 773 K to 95% at 973 K). At 7.5×10^{-4} mole fraction of TTIP, direct adsorption of TiO_2 monomers represented 54% of the total surface deposition rate at 773 K, increasing to 83% at 973 K.

We have found that, at low precursor concentration, the mole fraction of TiO_2 represented a maximum of 1% of the amount of TTIP depleted in the gas phase and the deposition was mainly by direct adsorption of the TTIP. This suggests that at low inlet precursor concentration, most of the TiO_2 monomers were swept away from the reactor, while with increasing concentration, a higher fraction of monomers could reach the substrate. This means that for all the conditions investigated here, the mass transfer to the substrate was the slowest step in the deposition, i.e., the reactor was working in a diffusion-limited regime. In a

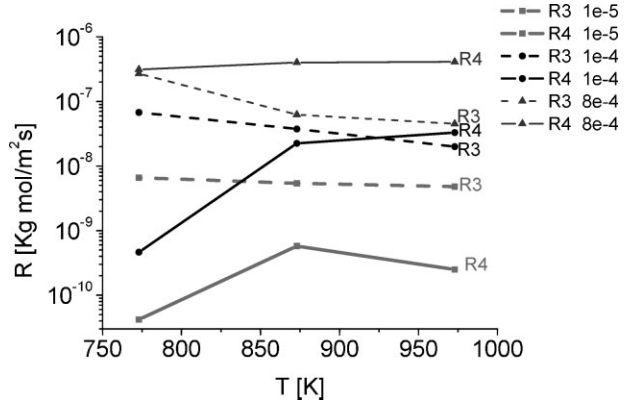

Fig. 7. Surface reaction rates as a function of substrate temperature and for various TTIP mole fractions. The rates of direct adsorption of TTIP and TiO_2 (i.e., R3 and R4) are represented by the dashed and solid lines, respectively.

previous work,[23] it was found that at a TTIP inlet concentration of 0.1% the transition from kinetic to diffusive regime occurred at substrate temperature of 723 K. In other work,[19] where a cold-wall reactor operating under similar conditions as in the current work was studied, it was found that the onset of the homogeneous decomposition of TTIP, and hence the switch from kinetic to diffusive regime, occurred at higher temperatures, in the range 873 - 923 K, for a precursor mole fraction of 3.8×10^{-5} to 4.5×10^{-4}. However, when water was added at the inlet, in the same proportion as the precursor, the onset temperature for the TTIP gas phase decomposition decreased to 723 K. A reason for the quantitative disagreement between those experimental data and our calculated results can be an overestimation of the depletion of TTIP due to the hydrolysis reaction. The activation energy and pre-exponential factor for the hydrolysis reaction of TTIP available in the literature,[20] were determined at 673 K and based on rather high initial water to TTIP ratios (ten times or higher). In the present simulation the water was obtained only as a by-product of the TTIP thermal decomposition, and the rate coefficients depended on the experimental conditions under which they were determined.[34]

3.3.1. Influence of the Temperature and Precursor Concentration

The TiO_2 net deposition rate increased with the rise of precursor concentration and decreased with the increase of substrate temperature (see Fig. 6) under all conditions investigated here.

The rising trend with precursor concentration is logical. The decreasing trend with increasing substrate temperature is a bit unexpected, but can be explained, based on the thickness of the boundary layer (Δ) and its dependence on the Reynolds number (Re).[35] Indeed, Δ was inversely proportional to the square root of Re. Re decreased with increasing temperature (T) at constant fluid mass density, i.e., $\Delta \propto 1/\sqrt{\mathrm{Re}} \propto T$. Indeed, a high temperature corresponded to a low Re and hence to a larger boundary layer. Therefore, the molecules responsible for the film growth, i.e., TTIP and TiO_2, could be swept by the radial flow early in space before they could reach the substrate by diffusion. On the other hand, at low substrate temperature, Re increased, and the layer became thinner. Consequently, the film growth molecules had to diffuse over a shorter distance to reach the substrate, and they could more easily contribute to the film growth.

Experimentally, a drop in the deposition rate with the rise of the temperature, in the temperature range where no particles are formed yet, has also been observed for low pressure MOCVD in several works,[3,13,36] and it was suggested that the deposition rate began to decrease with the temperature as soon as the gas-phase dissociation of TTIP had started. Besides the effect of temperature, the effect of the inlet TTIP concentration on the growth rate has

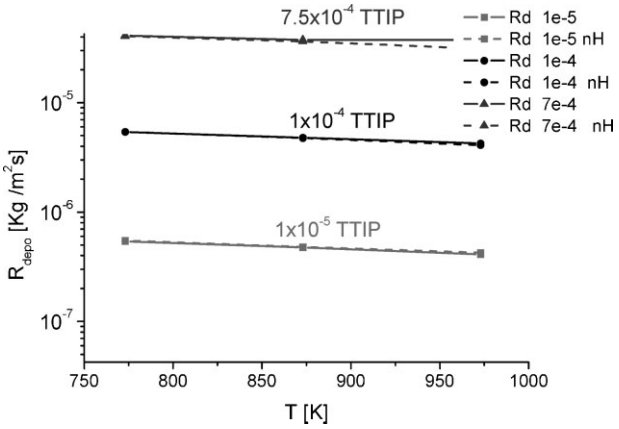

Fig. 8. Comparison of the deposition rates as a function of temperature and for different TTIP mole fractions, with (solid lines) and without (dashed lines) considering hydrolysis.

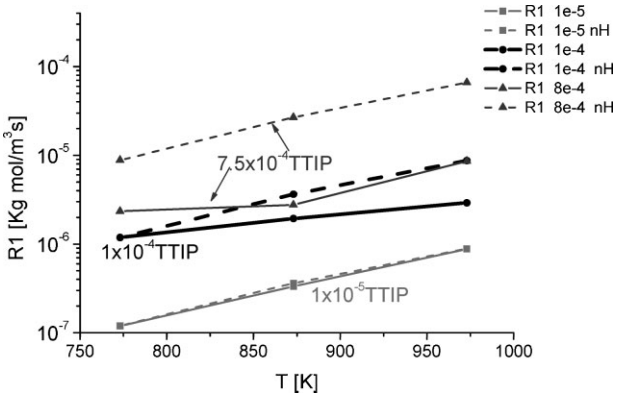

Fig. 9. Comparison of the TTIP homogeneous thermal decomposition rates, as a function of substrate temperature and for various TTIP mole fractions, calculated with (solid lines) and without (dashed lines) considering hydrolysis.

also been investigated,[13] and it was found that the growth rate increased with precursor concentration. Our calculated growth rates as a function of precursor concentration (see Fig. 6) are in very good agreement with the experimental rates previously reported,[17] which varied from 0.01 μm min^{-1} at 3.8×10^{-5} to 200 μm min^{-1} at 4.5×10^{-4} mole fraction of inlet precursor concentration. However as mentioned before, our calculations predicted that the deposition rate decreased in the temperature range investigated here, i.e., from 773 K to 973 K, while it was observed that the film growth rates began to decrease at temperatures higher than 873 K.

3.3.2. Influence of Hydrolysis

In the gas phase, the TTIP depletion was due to its thermal decomposition and hydrolysis. From Figure 4 we can see that at low precursor concentration, the hydrolysis and thermal decomposition rates are in the same order of magnitude, but as the concentration of TTIP increased, the hydrolysis became four orders of magnitude faster than the thermal decomposition. Thus we expect that under those conditions its influence is stronger.

As appears from Figure 8, the absolute value of the calculated deposition rate does not change considerably whether the hydrolysis reaction is included or not. However, hydrolysis promotes the depletion of TTIP and it is a much faster reaction than the thermal decomposition. Hence the hydrolysis will increase the monomer concentration, particularly at higher mole fraction of the precursor, and consequently the surface deposition rate by monomers will also increase.

For example as shown in Figure 9, at 10^{-5} mole fraction of TTIP, the homogeneous thermal decomposition rate, calculated when hydrolysis is included in the model (solid lines), or without hydrolysis (dash lines) are similar.

Consequently, the monomer concentration and the surface deposition rate by direct adsorption of monomers stays almost the same. Indeed, at 973K substrate temperature, the TiO_2 mole fraction increased from 9.91×10^{-8} to 1.01×10^{-7} when hydrolysis was considered, which represents a rise of only 8%. At a TTIP mole fraction of 7.5×10^{-4}, the calculated thermal decomposition rate is

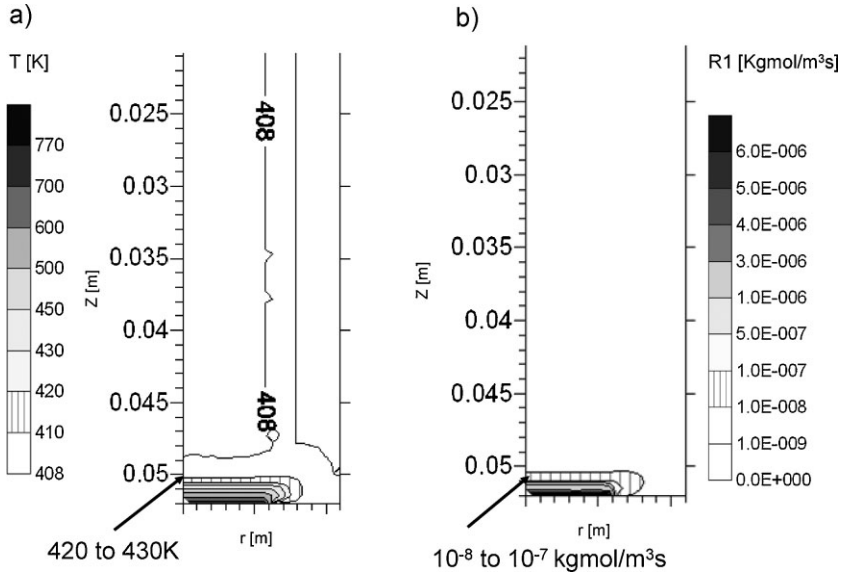

Fig. 10. Details of the a) temperature and b) TTIP homogeneous thermal decomposition rate profiles, at a substrate temperature of 773 K and TTIP mole fraction of 7.5×10^{-4}, when hydrolysis is not considered. Note that the isotherm corresponding to 408 K, (i.e., the temperature of the gas at the inlet), is found at $z = 4.87$ cm, i.e., at a distance from the substrate surface of 3.3 mm, and when hydrolysis was considered it was found at a distance of 2.5 mm.

around one order of magnitude lower than the rate calculated without hydrolysis. For example at a substrate temperature of 973 K, when both reactions (R1 and R2) were included in the model, the TiO_2 mole fraction increased 63 times (i.e., from 7.9×10^{-6} to 4.4×10^{-4}), and the surface deposition by direct adsorption of monomers rises 3 times, when compared to the calculations without hydrolysis.

In Figure 10 it can be observed that when the hydrolysis reaction was not considered in the model, the thermal decomposition of TTIP began to occur at $z = 5.05$ cm, i.e., at a distance of 1.5 mm from the substrate. This is closer to the substrate and at a region of higher temperature, when compared with the case in which the hydrolysis reaction is taken in account. Indeed, by comparing the contour lines of the thermal decomposition rate (Fig. 10b) with the temperature profile in Figure 10a, we can estimate that the onset temperature for this process is around 425 K, while it was around 415 K when hydrolysis was considered (see Fig. 3). Therefore we can conclude that when hydrolysis is taken into account in the model, the onset temperature for initiating the thermal decomposition of the precursor in the gas phase decreases slightly. This result agrees well with the experimental observation that when water is added the depletion of TTIP begins at lower temperatures.[11,19,37] For example it has been reported[19] that when water is added at the reactor inlet, the reactivity of the gas mixture increases (compared when water was not added), leading to the deposition of the TiO_2 film at lower temperatures.

4. Conclusions

The atmospheric MOCVD of thin TiO_2 films using TTIP as precursor and nitrogen as a carrier gas was simulated by means of CFD. The influence of the substrate temperature, precursor concentration, and occurrence of the hydrolysis reaction on the film growth was investigated. It was found that the temperature gradient was concentrated in the region just in front of the substrate surface; the surface deposition was uniform for all the conditions, whilst the net deposition rate increased with the precursor concentration and the decrease of the substrate temperature. At a mole fraction of TTIP of 10^{-5}, direct adsorption of TTIP was almost completely responsible for the film growth, while for a mole fraction of TTIP of nearly 10^{-3}, the TiO_2 monomer deposition became more important. Furthermore, it was found that the hydrolysis reaction of TTIP decreased slightly the onset temperature of the gas-phase thermal decomposition and increased the monomer production. Our calculated results are consistent with experimental observations reported in the literature.

5. Appendix

Table 2 provides the values for the molecular weight (Mw), the specific heat capacity at constant pressure (C_p), and the standard state enthalpy for each species considered in the model.

Table 2. Thermochemistry data for all the species considered in the model (the reference temperature for all the data is 298.15 K).

	Species	Molecular weight [kg kmol^{-1}]	Specific heat capacity [J kg^{-1} K^{-1}]	Standard state enthalpy [J kmol^{-1}]
1	$Ti(OC_3H_7)_4$	284.215	1.257[a]	-1.5079×10^{9}[b]
2	C_3H_7OH	60.095	1425.5[b]	-2.56×10^{8}[b]
3	C_3H_6	42.081	1440[c]	2.0441×10^{7}[c]
4	H_2O	18.015	2014[c]	-2.4184×10^{8}[c]
5	TiO_2(gas)	79.866	691.84[b]	-3.0543×10^{8}[b]
6	TiO_2(solid)	79.866	691.84[b]	-9.3872×10^{8}[b]
7	N_2	28.013	1040.67[c]	0[b]

[a] Calculated based on the gas kinetic theory.
[b] NIST, http://webbook.nist.gov.
[c] Taken from the literature [18].

Due to the small concentration of TTIP in the carrier gas, the mass diffusivity, viscosity, and thermal conductivity of the fluid mixture were taken as constant and equal to those of the nitrogen gas, as proposed by Nami et al.[22] The heat capacity for the gas mixture was calculated as the mass fraction average of the pure species heat capacities ($c_p = \sum Y_i c_p, i$) and the gas mixture density (ρ) was calculated based on the ideal gas law for an incompressible gas

$$\rho = \frac{P}{RT \sum Y_{i/} Mw_i}$$

where R is the universal gas constant, P the pressure, Y_i is the mass fraction of each species, which was calculated in FLUENT, through the solution of the continuity equation for the i^{th} species.

Received: April 8, 2008
Revised: August 12, 2008

[1] U. Diebold, *Surf. Sci. Reports* **2003**, *48*, 53.
[2] J. Hewitt, *Cosmet. Toiletries* **1999**, *114*, 59.
[3] K. H. Ahn, Y. B. Park, D. W. Park, *Surf. Coat. Technol.* **2003**, *171*, 198.
[4] K. Vydianathan, G. Nuesca, G. Peterson, E. T. Eisenbraun, A. E. Kaloyeros, *J. Mater. Res.* **2001**, *16*, 1838.
[5] A. Goosens, E. L. Maloney, J. Schoonman, *Chem. Vap. Deposition* **1998**, *4*, 109.
[6] I. K. Konstantinou, T. A. Albanis, *Appl. Catal. B: Environ.* **2003**, *42*, 319.
[7] A. Mills, N. Elliot, I. P. Parkin, S. A. O'Neill, R. J. Clark, *J. Photochem. Photobiol. A: Chem.* **2002**, *151*, 171.
[8] S. A. O'Neill, R. J. Clark, I. P. Parkin, N. Elliot, A. Mills, *Chem. Mater.* **2003**, *15*, 46.
[9] J. T. Brown, *Appl. Opt.* **2004**, *43*, 4506.
[10] T. Fujii, N. Sakata, J. Takada, Y. Miura, Y. Daitoh, M. Takano, *J. Mater. Res.* **1994**, *9*, 1468.
[11] A. Rathu, M. Ritala, *Chem. Vap. Deposition* **2002**, *8*, 21.
[12] S. I. Cho, C. H. Chung, S. H. Moon, *Thin Solid Films* **2002**, *409*, 98.
[13] H. Y. Lee, H. G. Kim, *Thin Solid Films* **1993**, *229*, 187.
[14] K. L. Siefering, G. L. Griffin, *J. Electrochem. Soc.* **1990**, *137*, 814.
[15] U. Backman, A. Auvinen, J. K. Jokiniemi, *Surf. Coat. Technol.* **2005**, *192*, 81.

[16] D. J. Won, C. H. Wang, H. K. Jang, D. J. Choi, *Appl. Phys. A* **2001**, *73*, 595.

[17] P. Babelon, A. S. Dequiedt, H. Mostefa, S. Bourgeois, P. Sibillot, M. Sacilotti, *Thin Solid Films* **1997**, *322*, 63.

[18] FLUENT, http://www.fluent.com.

[19] F. D. Dominica, *Surf. Coat. Technol.* **2004**, *188-189*, 225.

[20] T. Seto, M. Shimada, K. Okuyama, *Aerosol Sci. Technol.* **1995**, *23*, 183.

[21] S. Krumdieck, *Acta Mater.* **2001**, *49*, 853.

[22] Z. Nami, O. Misman, A. Erbil, G. S. May, *J. Cryst. Growth* **1997**, *171*, 154.

[23] E. Neyts, A. Bogaerts, M. De Meyer, S. Van Gils, *Surf. Coat. Technol.* **2007**, *201*, 8838.

[24] O. Okuyama, R. Ushio, Y. Kousaka, R. Flagan, J. Seinfeld, *AIChE J.* **1990**, *36*, 409.

[25] G. A. Battiston, R. Gerbasi, M. Porchia, A. Gasparoto, in *Chemical Vapor Deposition–Proc. 14th Int. CVD Conf. and EUROCVD-11*, Vol. 97–25(Eds: M. Allendorf, C. Bernard), The Electrochemical Soc., Pennington NJ **1997**, p. 660.

[26] H. K. Versteeg, W. Malalasekera, *An Introduction to Computational Fluid Dynamics: The Finite Volume Method*, Longman, Malaysia **1998.**

[27] A. J. Chorin, *Math. Comp.* **1968**, *22*, 745.

[28] S. V. Patankar, *Numerical Heat Transfer and Fluid Flow*, McGraw-Hill, New York **1986.**

[29] T. J. Barth, D. Jespersen, *Technical Report AIEA-89-0366*, AIAA 27th Aerospace Space Sciences Meeting, Reno, Nevada, **1989.**

[30] FLUENT 6.3 User's Guide Manual, Chapter 14, http://www.fluent.com.

[31] D. L. Smith, *Thin-Film Deposition: Principles and Practice*, McGraw-Hill, New York **1995.**

[32] S. Chen, M. G. Mason, H. J. Gysling, G. R. Paz-Pujalt, *J. Vac. Sci. Technol. A* **1993**, *11*, 2419.

[33] H. Komiyama, T. Kanai, H. Inoue, *Chem. Lett.* **1984**, *8*, 1283.

[34] S. Tsantilis, H. K. Kammler, S. E. Pratsinis, *Chem. Eng. Sci.* **2002**, *57*, 2139.

[35] H. O. Pierson, *Handbook of Chemical Vapor Deposition: Principles, Technologies and Applications*, William Andrew, New York **1999.**

[36] M. Okada, K. Tominaga, T. Araki, S. Katayama, Y. Sakashita, *Jpn. J. Appl. Phys.* **1990**, *29*, 718.

[37] W. Haenni, H. E. Hintermann, D. Morel, A. Simmen, *J. Phys. Coll.* **1989**, *C5*, 401.

